1323

MARCH 1977 PPPL-1323

SPECTROSCOPIC MEASUREMENTS OF ION TEMPERATURE IN ATC TOKAMAK WITH RF AND NEUTRAL BEAM HEATING

BY

S. SUCKEWER AND E. HINNOV

PLASMA PHYSICS LABORATORY

PRINCETON UNIVERSITY
PRINCETON, NEW JERSEY

This work was supported by U. S. Energy Research and Development Administration Contract E(11-1)-3073. Reproduction, translation, publication, use and disposal, in whole or in part, by or for the United States Government is permitted.

DISCLAIMER

NOTICE

Printed in the United States of America.

Available from
National Technical Information Service
U. S. Department of Commerce
5285 Port Royal Road
Springfield, Virginia 22151
Price: Printed Copy $ * ; Microfiche $3.00

*Pages	NTIS Selling Price
1-50	$ 4.00
51-150	5.45
151-325	7.60
326-500	10.60
501-1000	13.60

Spectroscopic Measurements of Ion Temperature in ATC Tokamak with RF and Neutral Beam Heating

S. Suckewer and E. Hinnov
Plasma Physics Laboratory, Princeton University
Princeton, New Jersey 08540

March 1977

PPPL-1323

SPECTROSCOPIC MEASUREMENTS OF ION TEMPERATURE IN ATC TOKAMAK WITH RF AND NEUTRAL BEAM HEATING

S. Suckewer and E. Hinnov

Plasma Physics Laboratory
Princeton University
Princeton, New Jersey 08540

ABSTRACT

Measurements of ion temperatures in the ATC Tokamak by means of Doppler broadening of various ion lines are described, and typical results presented for the various auxiliary heating experiments: compression, neutral beam, lower hybrid and ion cyclotron frequency heating. Radial resolution of the temperature measurements is achieved by utilizing spectrum lines of ions of different ionization potentials: OVII λ1623Å, CV λ2271Å and CIV λ1548Å, which are emitted from regions of different electron temperature. Measurement at a given radial location is performed as a function of time by repeated scanning of the line contour in times 1.5 - 3.0 msec. The results indicate variations of heating efficiency with location and with power input level.

I. INTRODUCTION

In order to determine the ion temperature in tokamak discharges, three experimental methods have been generally used: 1) measurement of the energy spectrum of neutral hydrogen or deuterium atoms emitted from the plasma in the energy range $\gtrsim$ 400 eV ("charge-exchange temperature"); 2) measurement of the neutron flux in deuterium plasmas ("neutron temperature"); and 3) measurement of spectral distribution of various impurity ion lines in the plasma ("doppler temperature"). Each of these methods has distinct advantages and disadvantages, and in general they tend to be complementary rather than competitive measurements of the behavior of ion temperature in time and space. In the present paper we present an account of the doppler temperature measurements in the ATC tokamak discharges under a variety of plasma heating methods.

The Adiabatic Toroidal Compressor (ATC) tokamak [1,2], as its name implies, can produce significant plasma heating by major-radius compression of the usual ohmically heated plasma in times comparable or smaller than the energy replacement time τ_E (usually several msec.). Additional power input, in quantities comparable to the ohmic power, has been provided by wave heating, either in the lower hybrid (LH) or the ion cyclotron range of frequencies (ICRF), and also by neutral beam (NB) heating.

Such auxiliary heating methods tend to produce substantial distortions to a Maxwellian energy distribution of the ions. It is a particular advantage of the doppler profile measurements that these still provide a measure of the average kinetic energy of the bulk of the ions under such conditions, in contrast to the other methods mentioned above that are strongly influenced by the high-energy tail of the distribution.

In a plasma with strong electron temperature gradients, the various states of ionization of atoms that are not completely stripped of electrons tend to be distributed spatially according to their ionization potentials, as will be described below. Thus, measuring the doppler temperature of different ions automatically provides spatial resolution of the ion temperature. However, finding suitable ion lines, especially in the hotter regions of the plasma (which implies ions of large ionization potential) is difficult. The strongest lines of all multiply ionized atoms lie in the far ultraviolet and x-ray region, whereas for the high-resolution doppler width measurements, longer wavelength lines have great advantages: in the Schumann region and above, $\lambda \gtrsim 1100\text{Å}$, it is possible to use transmission as well as reflection optics. This greatly facilitates the measurements by increasing the choice of experimental techniques. Moreover, the doppler widths are proportional to the wavelength, thus the half-intensity width $\Delta\lambda_D$ is

$$\Delta\lambda_D/\lambda = 2.43 \times 10^{-3} (T_i(\text{keV})/M_i)^{1/2} \qquad (1)$$

for a Maxwellian distribution, with M_i the atomic weight of the ion.

In principle, one can add small quantities of various elements to the discharge in order to increase the available choice of appropriate lines. However, in the present paper we have used only the spontaneously occurring oxygen and carbon lines: the λ 1623Å line of OVII (ionization potential 739 eV). the λ 2271Å line of CV (E_i = 392eV) and λ 1548Å of CIV (E_i = 64eV). These are sufficient to provide a reasonable indication of the behavior of T_i on the ATC discharges.

II. EXPERIMENTAL ARRANGEMENT

The line profiles were measured by means of a 1 meter Ebert-Fastie type Jarrell-Ash monochromator, equipped with a rotating LiF plate in front of the exit slit. (This scheme has evolved by various adaptations from the instrument described by Hirschberg and Wilson [3]). The monochromator is air-tight, filled with argon to about 1.2 atmospheres, and connected to the tokamak vacuum vessel by means of a LiF window as shown in Fig. 1. The 1200 line/mm grating was used near the blaze angle: in the 7th order for the λ 1548Å and λ 1623Å lines and 5th order for the λ 2271Å line. The detectors were either of two photomultipliers (to minimize stray light, overlapping orders, etc.): an EMR tube with LiF windows and CsI cathode for $\lambda < 2100$Å or an RCA quartz-window, S-19 photocathode tube for $\lambda > 2000$Å. The instrumental profile (bandwidth), determined mostly by the entrance and exit slits, was sufficiently close to a Gaussian to allow expressing ion temperature by

$$T_i = K(\Delta\lambda_M^2 - \Delta\lambda_{IN}^2)/\lambda^2 \qquad (2)$$

with $\Delta\lambda_M$ and $\Delta\lambda_{IN}$ the measured and instrumental half-intensity widths, and K a constant proportional to the mass of the ion. In most measurements the instrumental width was chosen small compared to the measured width ($\Delta\lambda_{IN}/\Delta\lambda_M \approx 0.2\text{-}0.3$). The Zeeman splitting of the lines was small compared to the doppler width, and could be accounted for by minor adjustments to $\Delta\lambda_{IN}$.

In earlier measurements the LiF plate was stationary, and was rotated between discharges through small angles. Thus, about 20 discharges were required to determine the profile (as a function of time during the discharge). Samples of such measurements, at a particular time in the discharge, are shown in Fig. 2 for the CIV and OVII lines. The dashed curve is a Gaussian with the same half-intensity width as the measured curve. The points furthest right are background levels, measured about two half-widths further out from the center.

Recently, a rapid scan feature has been added to the system: a vibrating LiF plate that scans the spectrum line repeatedly with a period of about 2.5-3.5 msec. If T is the period of vibration and Φ_o the maximum angle of the plate of thickness ℓ and index of refraction $n(\lambda)$, the wavelength varies in time as

$$\Delta\lambda(t) = \lambda(t)-\lambda(0) = \ell\frac{\delta\lambda}{\delta\chi}\sin(\Phi_o \sin t/T)\left[1 - \left(\frac{1-\sin^2(\Phi_o \sin t/T)}{n^2-\sin^2(\Phi_o \sin t/T)}\right)^{\frac{1}{2}}\right] \quad (3)$$

where $\delta\lambda/\delta\chi$ is the reciprocal dispersion of the monochromator, and $\lambda(0)$ is the wavelength at the time the plate is

perpendicular to the light direction. This latter wavelength may be chosen to coincide with the intensity maximum by rotating the grating. Then near the intensity maximum the wavelength varies linearly with time,

$$\Delta\lambda(t) \approx \ell \frac{\delta\lambda}{\delta\chi}\left(1 - \frac{1}{n(\lambda)}\right)\frac{\Phi_o}{T}\, t \qquad (4)$$

Samples of typical rapid-scan signals are shown on Fig. 3 for the OVII λ1623Å and CV 2271Å lines taken during RF heating experiments. Also shown in Fig. 3 is the effective instrumental profile obtained in the first order with the HgI 4354Å line from a low pressure mercury lamp. The instrumental profile is determined largely by the 200μm entrance and exit slits.

This rapid-scan system allows T_i measurements during one discharge, thus eliminating the demand of detailed shot-to-shot reproducibility of the discharge, which was difficult to achieve, especially in the case of high-power RF heating. The system thus allows observation of changes in the ion temperature behavior as the RF heating conditions were changed, thus facilitating the search for optimum heating conditions.

The same measurement system has been used in ion temperature [4] and plasma rotation [5] measurements in the ST tokamak, and in impurity ion concentration measurements [6] in the ATC.

III. RADIAL DISTRIBUTION OF DOPPLER TEMPERATURE

During the quasisteady phase of tokamak discharges, the light emitted by various ions originates largely from radial shells with thicknesses small compared to the plasma (limiter) radius. The location and thickness of such shells is determined primarily by the electron temperature profile and the ionization potential (hence, ionization time) of the ion, and modified somewhat by the radial drift velocity of the ions. The doppler temperature measured from a particular ion light, thus refers to the corresponding shell radius.

In order to understand the formation of such shells, we note first that the radial ion drift velocity $v_\perp$ must be of the order of limiter radius, a , divided by particle confinement time, or typically 1-3 cm/msec . The radial velocity may vary somewhat with radius, and with different plasma conditions, but this will not change the picture except in quantitative detail.

Secondly, the electron temperature and density radial profiles in tokamak discharges also have characteristic shapes that vary only in detail - roughly parabolic for $N_e(r)$ and considerably sharper (often resembling the square of the density profile) for $T_e(r)$. Typical shapes of measured profiles in an ATC discharge are shown in Fig. 4. Also shown in Fig. 4 are the ionization times

$$\tau_{ion} = [N_e S_i(T_e)]^{-1} \qquad (5)$$

for various carbon and oxygen ions at the experimental N_e, T_e. The rate coefficients S_i are not too precisely known [7], but again this does not greatly affect the picture: the ionization time typically drops from $\tau_{ion} \gg 10$ msec (practically no ionization) to $\tau_{ion} \ll 1$ msec (practically instantaneous ionization) within a range of radii $\Delta r \ll a$. Thus the inward boundary of ions drifting at a few cm/msec, must be fairly sharply defined. Only when the ionization potential of an ion, $E_i \gtrsim kT_e(0)$, the central electron temperature, such as in the case of OVII and OVIII ions in the above example, will it extend over a large radial range near the center of the plasma.

The horizontal lines in Fig. 4 show the approximate radial range of the various ions if they were to move inward (to the left) at a constant velocity of 2 cm/msec. Also shown in the case of the heliumlike ions OVII and CV is the range they would have in the case of coronal equilibrium (C.E.), i.e., no radial motion. Other radial velocities in the above-mentioned probable range will only slightly change these locations because of the steepness of the τ_{ion} curves.

The outward boundary of an ion range is more vague. Although some experiments [8,6] indicate that the outer boundaries are also fairly well defined, the reason for this is not well understood, since volume recombination is usually too slow to affect the profiles appreciably. However, even though the outward ion density range is not limited, the light emission drops outward because of the decrease of plasma density and

electron temperature. The local light emissivity is proportional to the ion and electron density and the excitation rate coefficient $S_x(T_e)$. At the ions drift outward from the radius where they are produced by ionization of inward moving atoms, their density drops because of the increased volume, and so does the electron density. These effects decrease the emissivity of all ions at increasing radii. However, in some cases, and particularly the λ1623 and λ2271 of the heliumlike OVII and CV ions a much more important effect is the decrease of $S_x(T_e)$ with the temperature drop: the effective excitation potential, from the ground state of the ion, for these lines is nearly equal to the ionization potential of these ions. Consequently, although the heliumlike ions are produced at relatively low temperature, the line-emission is concentrated toward the high-temperature end of the range. In Fig. 4 the shaded portions of the OVII and CV ranges show the range where more than half of the light of the λ1623 and λ2271Å lines is emitted, taking into account excitation as well as ionization rates.

Thus, in many cases of interest and, in particular, all cases mentioned in this paper, the ion light is fairly sharply concentrated near a radius that may be fairly adequately estimated by arbitrarily setting $v_\perp \tau_{ion}(r) = 1$ cm (i.e. a distance small compared to plasma radius). Because of the usual strong radius-dependence of τ_{ion}, neither the uncertainties

of $v_\perp$, nor the exact value of the above-mentioned condition affect the radius estimate sensitively. In the limit of small $v_\perp$, the corresponding radial locations may be found from coronal equilibrium. For very large $v_\perp$, the ions of course, are not well localized.

In the experiments described below, the location of the three lines, OVII λ1623Å, CV λ2271Å, and CIV λ1548Å are all approximately those given in Fig. 4, i.e. $r/a \approx 0.3, 0.5, 0.8$, respectively, with $a = 17$ cm in uncompressed plasmas. In compressed plasmas, the relative locations are expected to move somewhat outward, but because of the lack of detailed electron temperature measurements on the compressed state the changes are not quantitatively known. The charge-exchange temperatures (and even more the neutron temperatures) on the other hand generally measure the highest (central) ion temperature along the line of sight.

IV. EXPERIMENTAL RESULTS

Fig. 5 presents typical results of T_i measurements by means of the OVII line broadening, with and without neutral beam heating preceeding the compression. The discharge occurred in deuterium, with a ohmic heating toroidal current $I_{OH} \approx 60$ kA. In compression, the major radius, R, of the toroidal plasma was changed from 90 cm to 40 cm between 30-32 msec . The open circles show the ion temperature behavior without the neutral beam heating: a gradual increase before 20 msec levelling off

at about 200 eV, followed by roughly doubling during the compression and subsequent drop with a time constant of about 10 msec. The actual temperature rise during the compression may be somewhat larger, in fact close to the expected ratio of 2.8-2.9 for adiabatic compression, because of the hottest part of the discharge OVII becomes ionized and therefore, ceases to radiate. (The position of the radiation moves relatively further outward.) The crosses describe the ion temperature in a similar discharge with 60 kW neutral beam heating for 10 msec before compression. The additional heating results in a $\Delta T_i \approx 80$ eV . Whether the compressional increment is relatively less in this case is not clear from these data for the above-mentioned reason, but a few milliseconds after the compression the effects of the neutral beam seem to have disappeared. The dashed curve labelled "charge-exchange" temperature was measured on a different day in a somewhat similar discharge (but without compression). The quantitative agreement with the doppler temperature is fortuitous (when measured in the same discharge, the charge-exchange temperatures are always slightly higher), but the indicated change of T_i during the neutral beam heating is very similar. From such comparisons it appears that in the case of neutral beam heating, the charge-exchange method was an adequate means of ion temperature measurement, and most of the measurements in ATC were performed by charge-exchange. The results indicated a roughly linear increase of ΔT_i with beam power [9,10].

The first Lower Hybrid heating experiments were performed with two-waveguide, 180° nonadjustable phase difference coupling of 800 MHz power, up to 90 kW for 5 msec. Typical results of ion temperature measurements with and without the RF pulse are shown in Fig. 6 — OVII doppler and charge-exchange measurements near the center and CIV doppler measurements near the periphery. The first two measurements are in general agreement, although the shot-to-shot reproducibility, especially with RF heating on, was rather poor. The peripheral CIV temperature shows a significant decrease during the RF heating, i.e. the temperature profile narrows, qualitatively similarly to the ICRF heating results presented below. The intensity of the OVII line did not change appreciably with applied RF power, wheras the CIV line intensity increased markedly, indicating an increase of peripheral carbon and probably electron density.

A more versatile system - including a four-waveguide phase-adjustable power coupling [11], and the single-shot rapid line scan (Fig. 3) - was used to investigate the LH heating temperature changes in more detail. Fig. 7a shows the temperature change near the center ($r \simeq 0.3a$) as a result of a 5 msec 140 kW RF pulse, and Fig. 7b a similar change further out ($r \simeq 0.5\text{-}0.6a$) produced at lower power level. Clearly, the heating efficiency is better in the latter case. The behavior of ΔT_i at the CV radius ($\sim 0.5a$) with increasing power P_{RF} is depicted in Fig. 8a for $P_{RF} < 120$ kW. At power levels $\gtrsim 120$ kW the temperature increase diminished and disappeared entirely by

150 kW. Qualitatively similar results obtained for OVII ($r \approx 0.3a$), but at somewhat higher power levels: ΔT_i disappeared only at power levels > 160kW . A change of heating efficiency at different plasma densities is shown in Fig. 8b. The power level variations of Fig. 8a refer to the higher plasma density, where the heating efficiency was optimum.

Adequate interpretation of ΔT_i drop for high RF power levels in terms of plasma processes does not seem feasible at present. However, it seems certain that changes in temperature and density profiles and probably plasma composition, caused by enhanced plasma-wall interactions, are heavily involved. This drop of ΔT_i is probably associated with an observed increase in density at the periphery of the plasma as a result of injection of impurities. Associated with the density increase an increase in reflection of the applied RF signal was observed. The power level at which this increased reflection takes place was found to depend on the condition of the ATC vacuum chamber and of the teflon window in the waveguide coupler. When the vacuum vessel and the teflon window were relatively clean about 1 kW/cm^2 could be transmitted in the coupling system, but the maximum power density had dropped by about one third by the time the experiment was terminated.

In ICRF heating experiments, 25 MHz power was applied to the plasma for 10 msec, at different power levels, the location of the ion cyclotron resonance layer being positioned by appropriate choice of toroidal field [12]. Fig. 9 shows a

typical change in the OVII doppler temperature at 50 kW power, with the resonant layer near the center at B_T = 16.5 kGauss. Changes of radial profiles of electron and ion temperatures caused by ICRF pulse are shown in Fig. 10. Both T_e and T_i profiles are distinctly narrower with RF power on. It is interesting to note that the peripheral CIV ion temperature is the same as the local electron temperature, presumably as a result of the relatively rapid electron-ion equilibration time. Thus, the peripheral cooling may be caused by either electrons (through increased radiation and ionization rate) or ions (through increased charge-exchange rate) if the recycling rate were increased. Also, since the total ohmic heating current remains constant, the increased peripheral resistivity implies higher current density and ohmic heating power near the center. Furthermore, the change of the current distribution also affects the rotational transformer and therefore could change the particle transport rate. Thus a number of indirect effects can affect the development of the ion temperature profile in addition to the direct power input by wave adsorption. Similar problems arose in the case of lower hybrid and neutral beam heating.

V. SUMMARY

A collection of measured ion temperature ("doppler temperature") changes, produced by various supplementary heating techniques on ATC tokamak, is shown in Fig. 11. The different

measurement methods imply different radial locations, as shown in Figs. 4 and 10.

Evidently, at power input levels considerably smaller than the ohmic heating power, the two wave heating methods and the neutral beam produce comparable heating at the same energy input. However, only the neutral beams heating in ATC has so far been able to apply high power (comparable to the ohmic heating), with continued linear increase of heating, in quantitative agreement with other experiments [13,14]. In wave heating other effects that have not been adequately determined but probably include prominently enhanced wall-interactions have limited either the power input level or its duration.

It is however, quite clear that for quantative interpretation of heating efficiencies with specialized techniques detailed information of spatial and temporal development of not only ion temperature, but also of electron temperature, density, and plasma composition is essential.

ACKNOWLEDGMENTS

The data reported here were obtained during auxiliary heating experiments in ATC, namely, neutral beam heating conducted by Drs. R. A. Ellis and H. P. Eubank, lower hybrid heating by Drs. W. M. Hooke, S. Bernabei, and R. W. Motley, ion cyclotron heating experiment by Dr. H. Takahashi. We are deeply indebted to all of them for effective cooperation and various interesting discussions. We also wish to express our gratitude to

Drs. C. C. Daughney, R. J. Goldston, H. Hsuan, R. R. Smith, and T. Nagashima for collaboration during measurements.

We thank M. R. Shoemaker and his technicians for their help in the operation of ATC.

This work was supported by the U. S. ERDA Contract E(11-1)-3073.

REFERENCES

[1] BOL, K., ELLIS, R. A., EUBANK, H. P., FURTH, H. P., JACOBSEN, R. A., JOHNSON, L. C., MAZZUCATO, E., STODIEK, W., TOLNAS, E. L., Phys. Rev. Lett. 29 (1972) 1945.

[2] BOL, K., CECCHI, J. L., DAUGHNEY, C. C., DEMARCO. F., ELLIS, R. A., EUBANK, H. P., FURTH, H. P., HSUAN, H., MAZZUCATO, E., SMITH, R. R., in Plasma Physics and Controlled Nuclear Fusion Research (Proc. 5th Int. Conf., Tokyo, 1974) 1, EAEA, Vienna (1975) 83.

[3] HIRSCHBERG, J. G., WILSON, E., Princeton PPL Report MATT-564 (1967) unpublished.

[4] DIMOCK, D., ECKHARTT, D., EUBANK, H. P., HINNOV, E., JOHNSON, L. C., MESERVEY, E., TOLNAS, E., GROVE, D. J., in Plasma Physics and Controlled Nuclear Fusion Research (Proc. 4th Int. Conf., Madison, 1971) 1, IAEA Vienna (1971) 451.

[5] JOBES, F. C., HOSEA, J. C., Proc. 6th European Conf. on CTR and Plasma Physics, Moscow, 1973, Vol. I, 199 .

[6] ELLIS, R. A., DAUGHNEY, C. C., HAWRYLUK, R. J., POST, D. E., SUCKEWER, S., TAKAHASHI, H., Bull. Am. Phys. Soc. 21 (1975) 1083.

[7] LOTZ. W., Astrop. J., Supplement 14 (1967) 207.

[8] TFR Group, Phys. Rev. Lett. 36 (1976) 1306.

[9] BOL, K., CECCHI, J. L., DAUGHNEY, C. C., ELLIS, R. A., EUBANK, H. P., FURTH, H. P., GODLSTON, R. J., HSUAN, H., JACOBSON, R. A., MAZZUCATO, E., SMITH, R. R., STIX, T., Phys. Rev. Lett. 32 (1974) 661.

[10] ELLIS, R. A., EUBANK, H. P., GOLDSTON, R. J., SMITH, R. R., NAGASHIMA, T., Nuclear Fusion 16 (1976) 524.

[11] HOOKE, W. M., BERNABEI, S., EUBANK, H. P., GOLDSTON, R. J., NAGASHIMA, T., MOTLEY, R. W., PORKOLAB, M., SUCKEWER, S., Bull. Am. Phys. Soc. 21 (1976) 1157.

[12] TAKAHASHI, H., DAUGHNEY, C. C., ELLIS, R. A., GOLDSTON, R. J., HSUAN, H., NAGASHIMA, T., PAOLONI, F. J., SIVO , A. J., SUCKEWER, S., Bull. Am. Phys. Soc. 21 (1976) 1157.

[13] LYON, J. F., Bull. Am. Phys. Soc. 21 (1976) 1071.

[14] TFR Group, Proc. 6th Int. Conf. on Plasma Physics and Controlled Nuclear Fusion, EAEA CIV/A4-2, Berchtesgaden (1976).

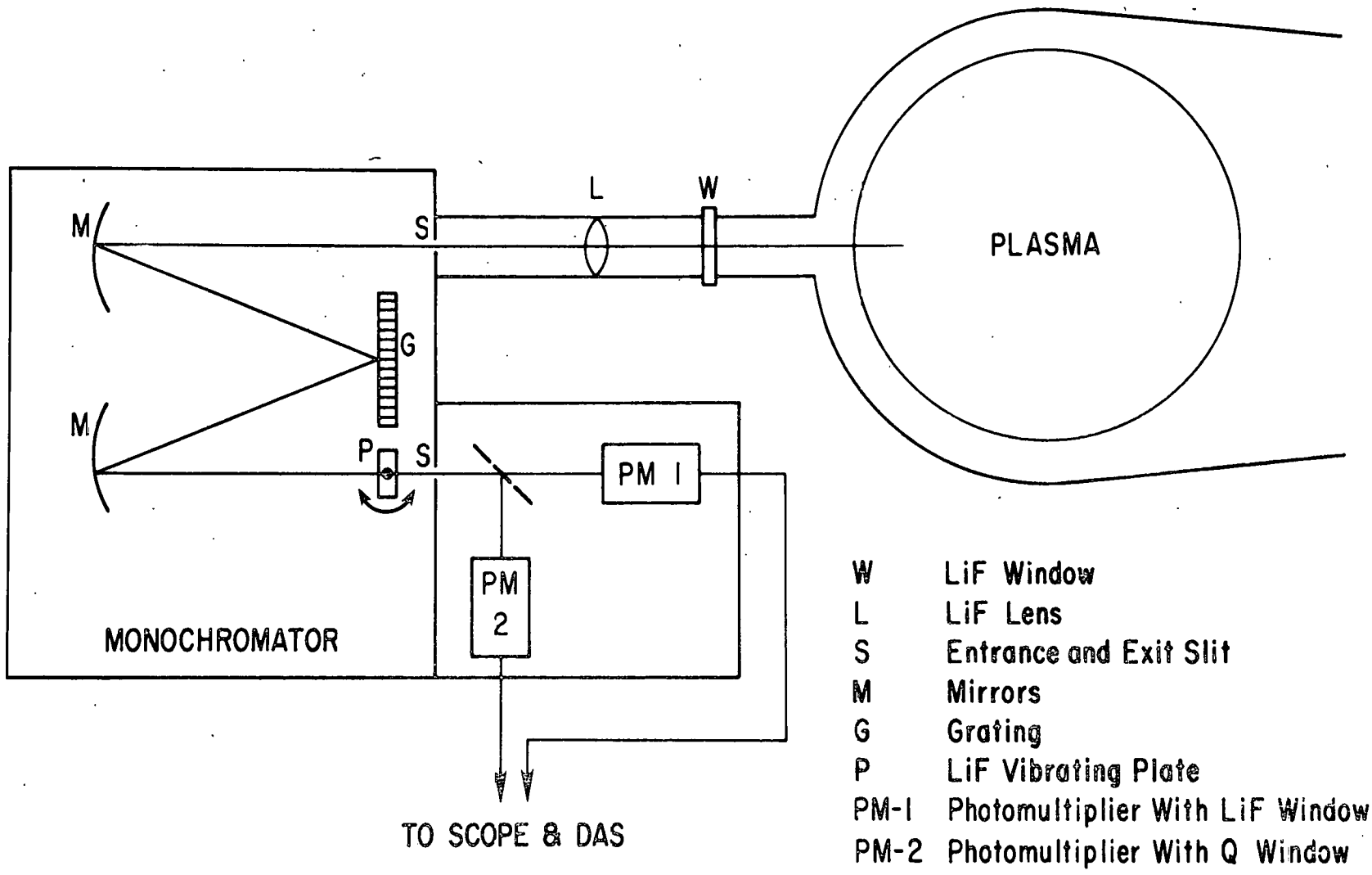

763735

Fig. 1. Diagram of spectrum line-scanning arrangement. DAS is the Data Accumulation System, which stores the data, averages over several shots if required, and computes the temperature $T_i(t)$ from Eq. 2.

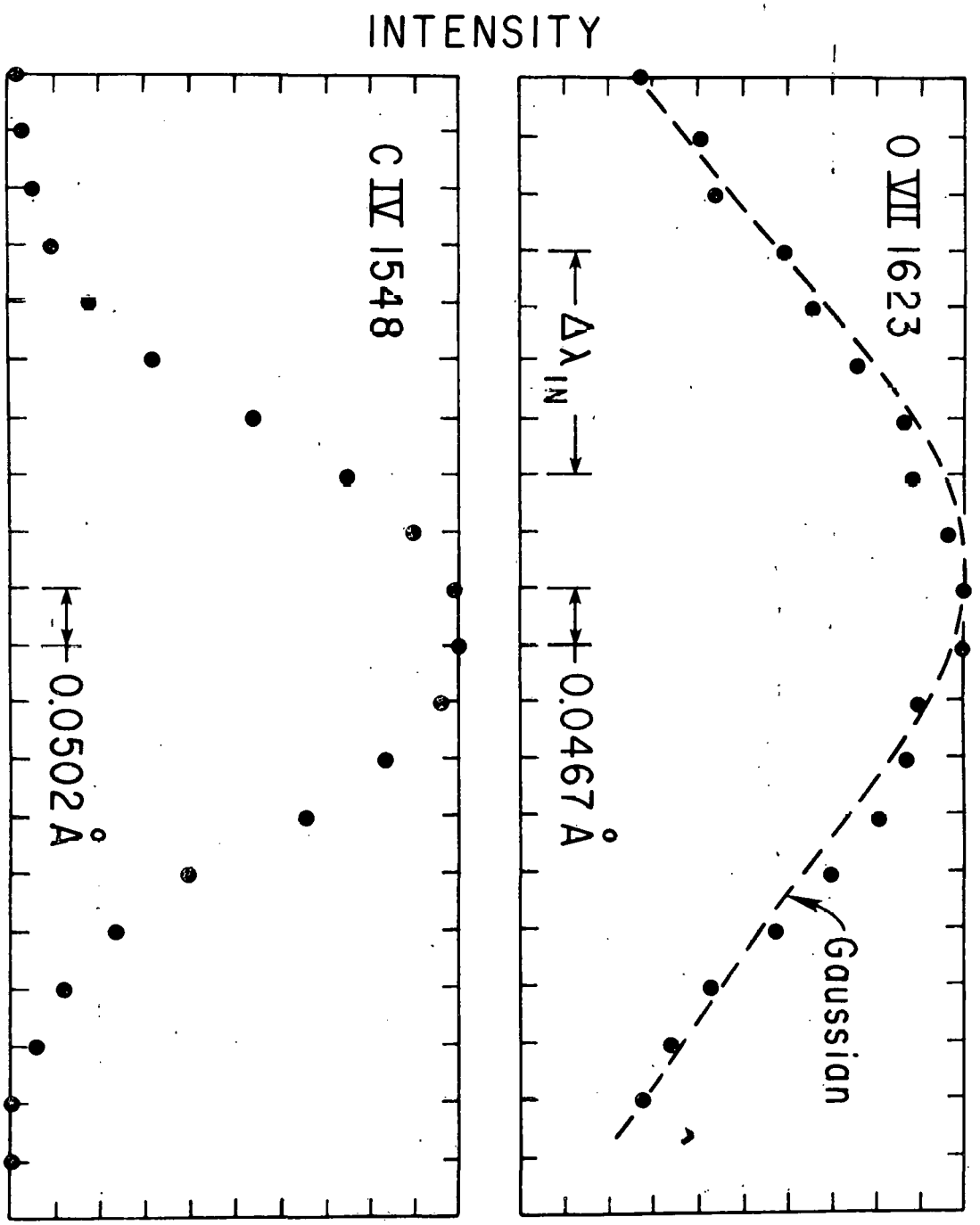

Fig. 2. Measured profiles of CIV 1548Å and OVII 1623Å lines taken by "shot by shot" scan. Abscissa unit 0.0467Å for OVII, 0.0502Å for CIV. Instrumental width 3.7 units in both cases.

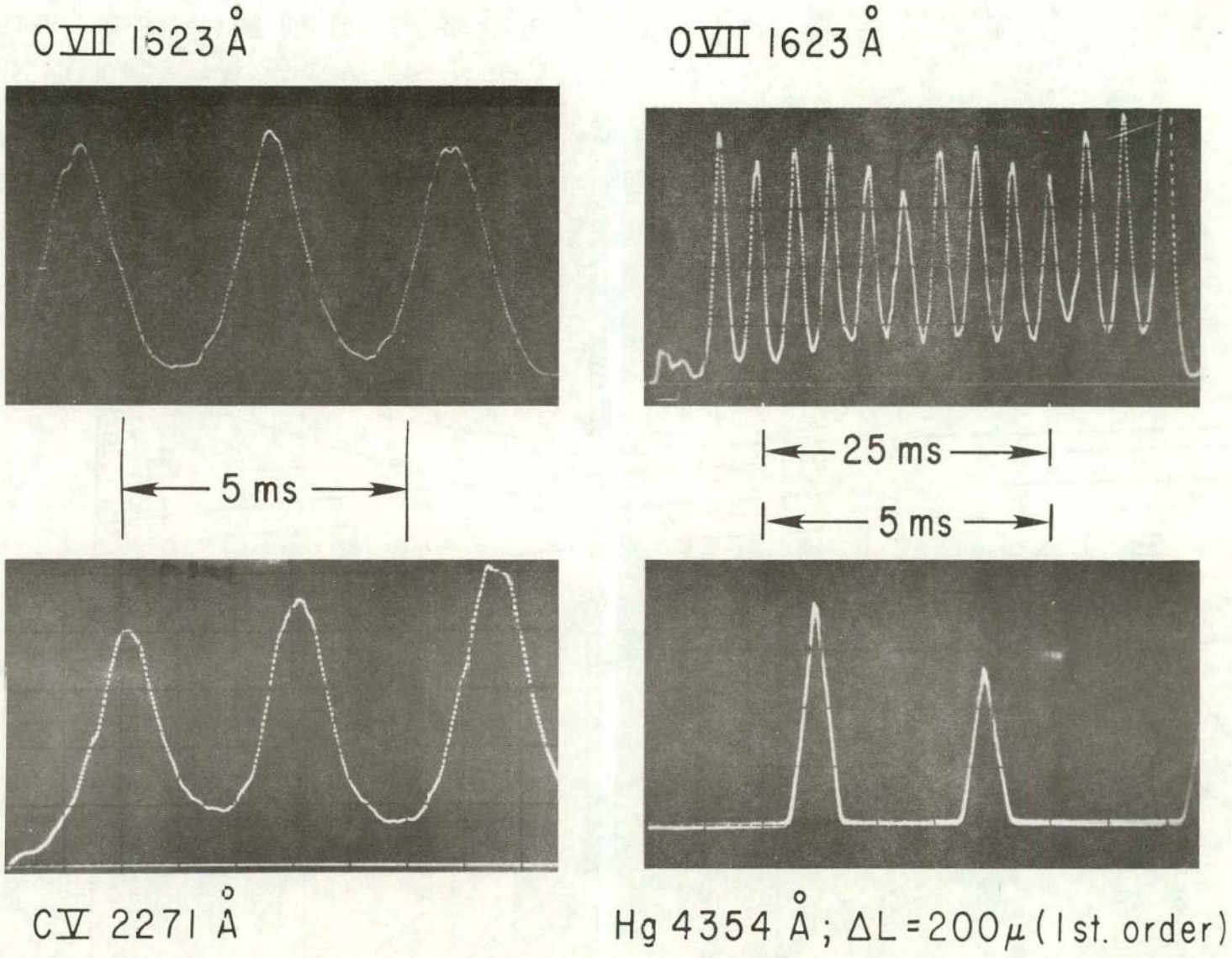

Fig. 3. Samples of fast-scanning signal for OVII, CV and CIV lines, and the instrumental profile.

773027

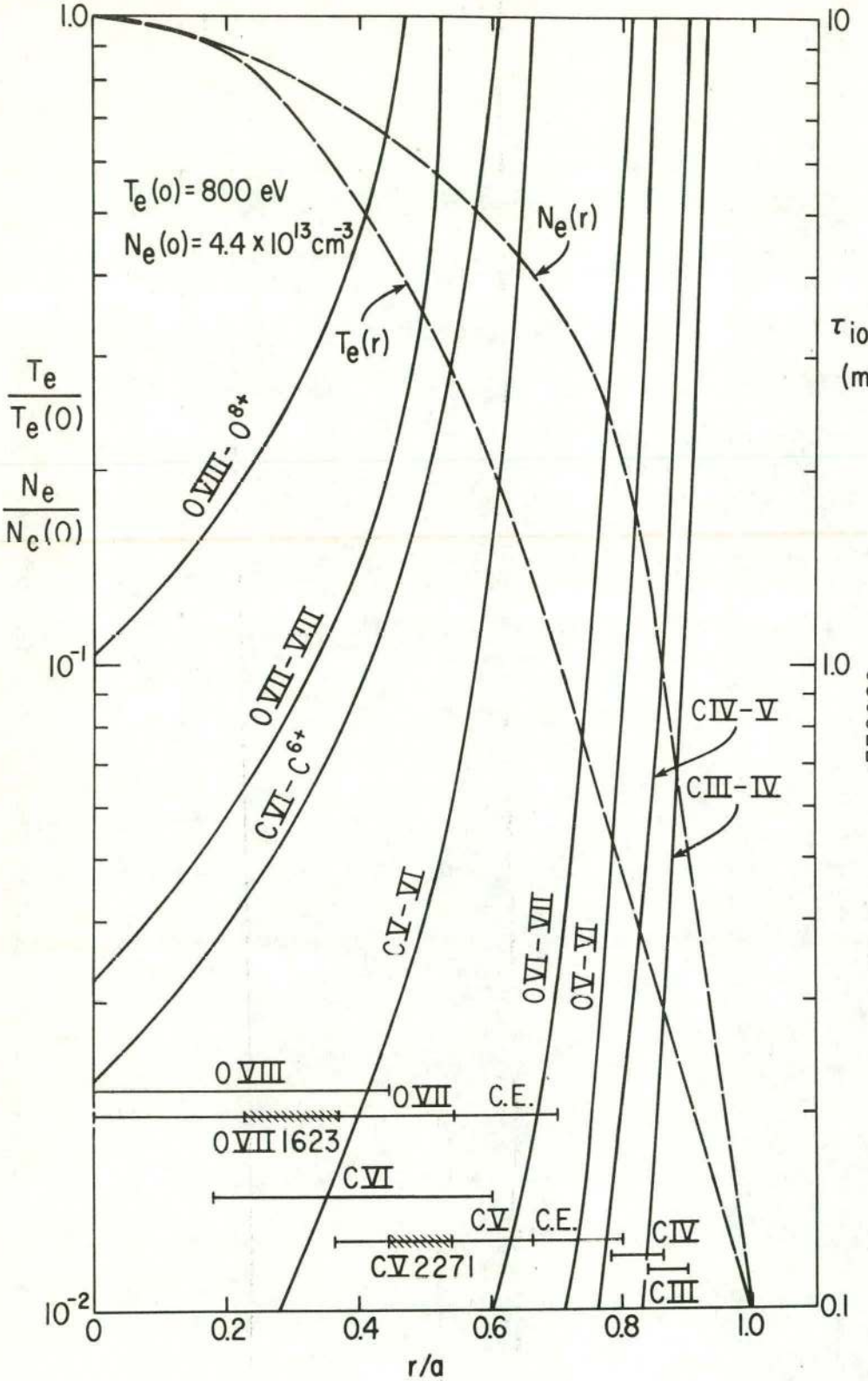

Fig. 4. Time of ionization (τ_{ion}) of carbon and oxygen ions of different stages of ionization as a function of plasma radius r . Expected positions of emission of lines CV λ2271Å, and OVII λ1623Å are indicated by shading on the horizontal lines, which indicate the radial range of the ions.

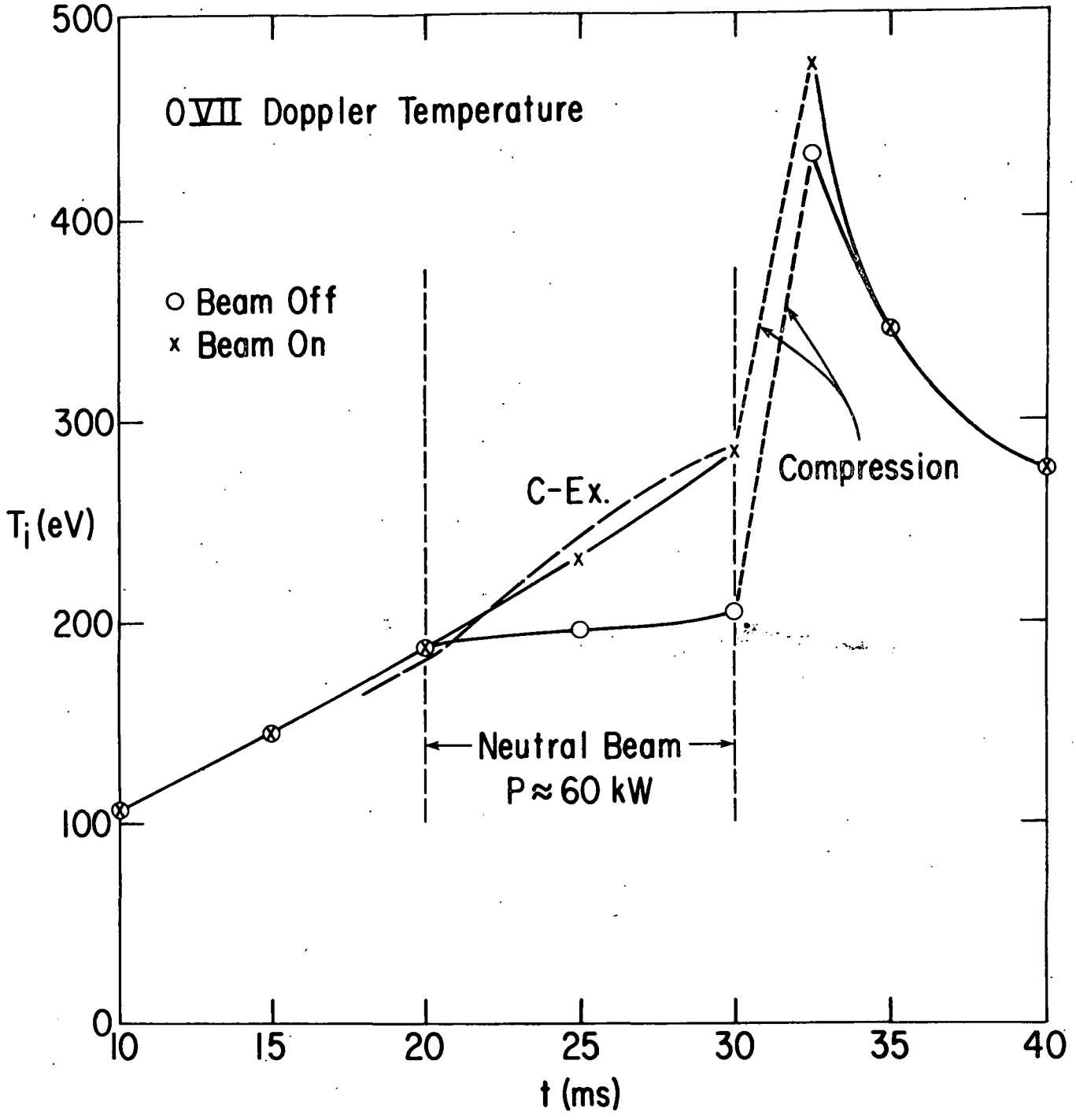

Fig. 5. Doppler T_i for plasma heated by compression with and without neutral beam.

766108

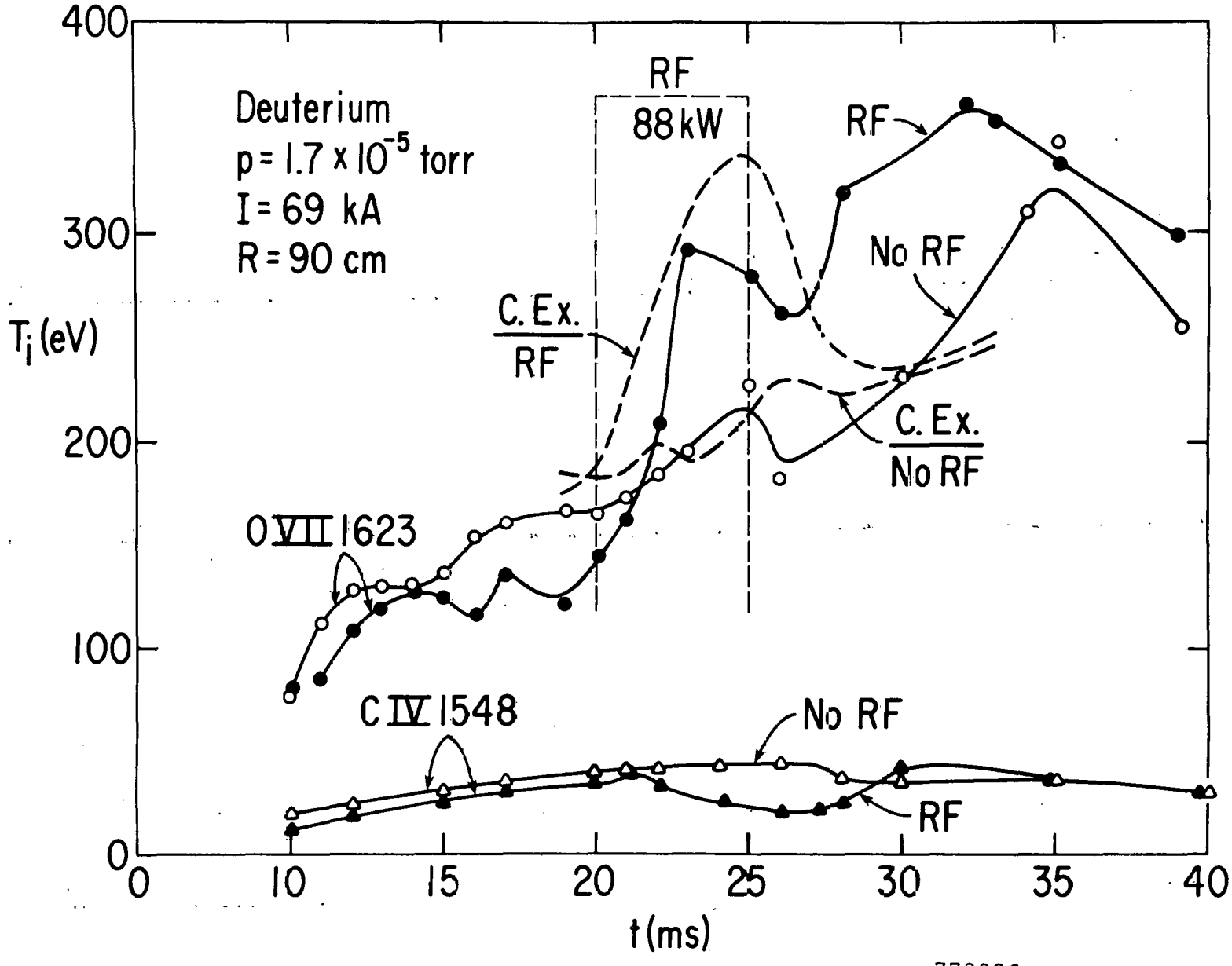

773026

Fig. 6. Doppler T_i ("shot by shot" measurements) for LH experiment with two waveguides coupling. Dashed curves give T_i from charge-exchange measurements.

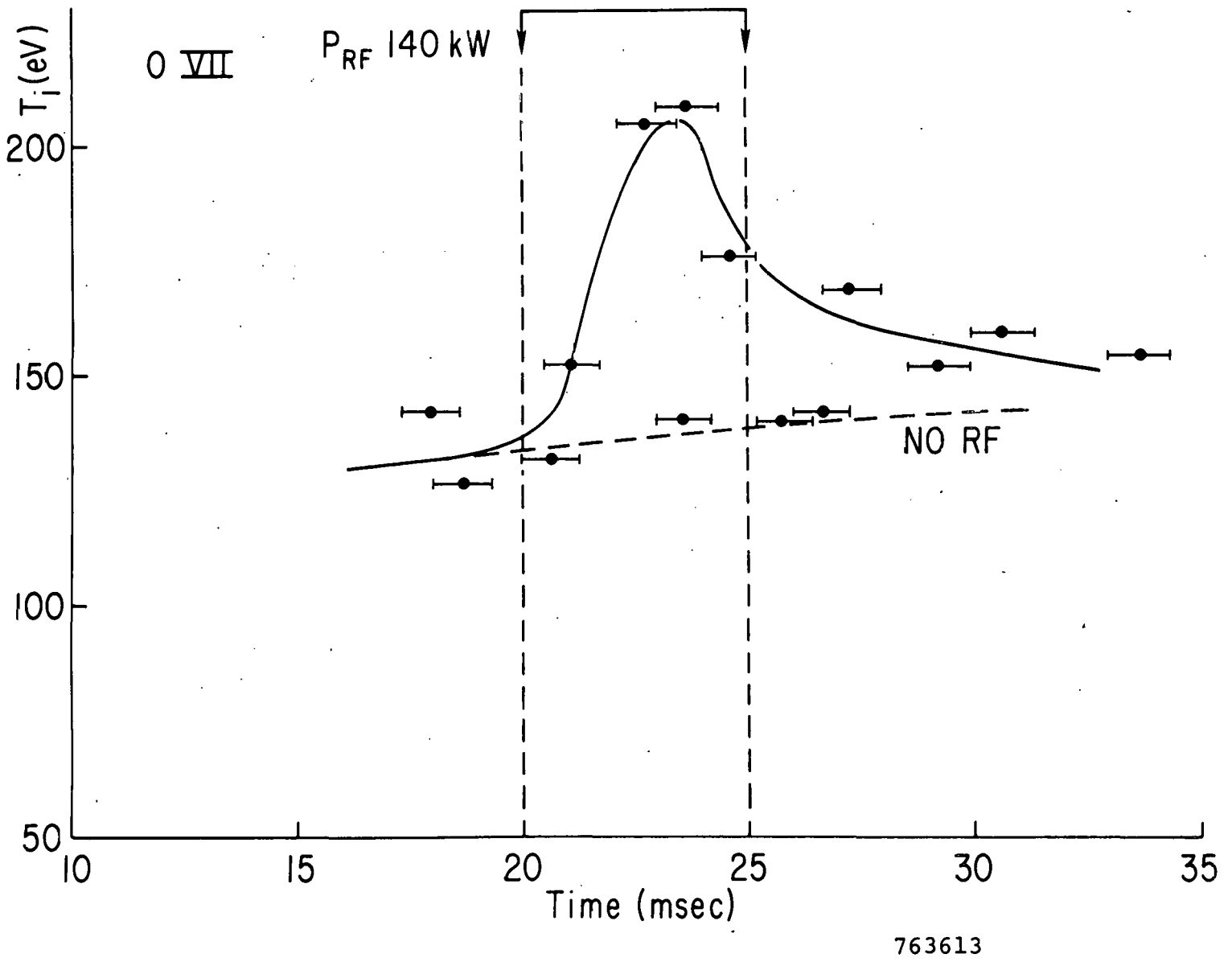

Fig. 7. Ion temperature for LH experiments with four waveguides coupling (rapid line-profile scanning). T_i from broadening of OVII 1623Å (RF power $P_{RF} \simeq 140$ kW) (a) and from broadening of CV 2271Å (RF 105≃kW) (b). Results for RF-power turn-off are indicated by "No-RF".

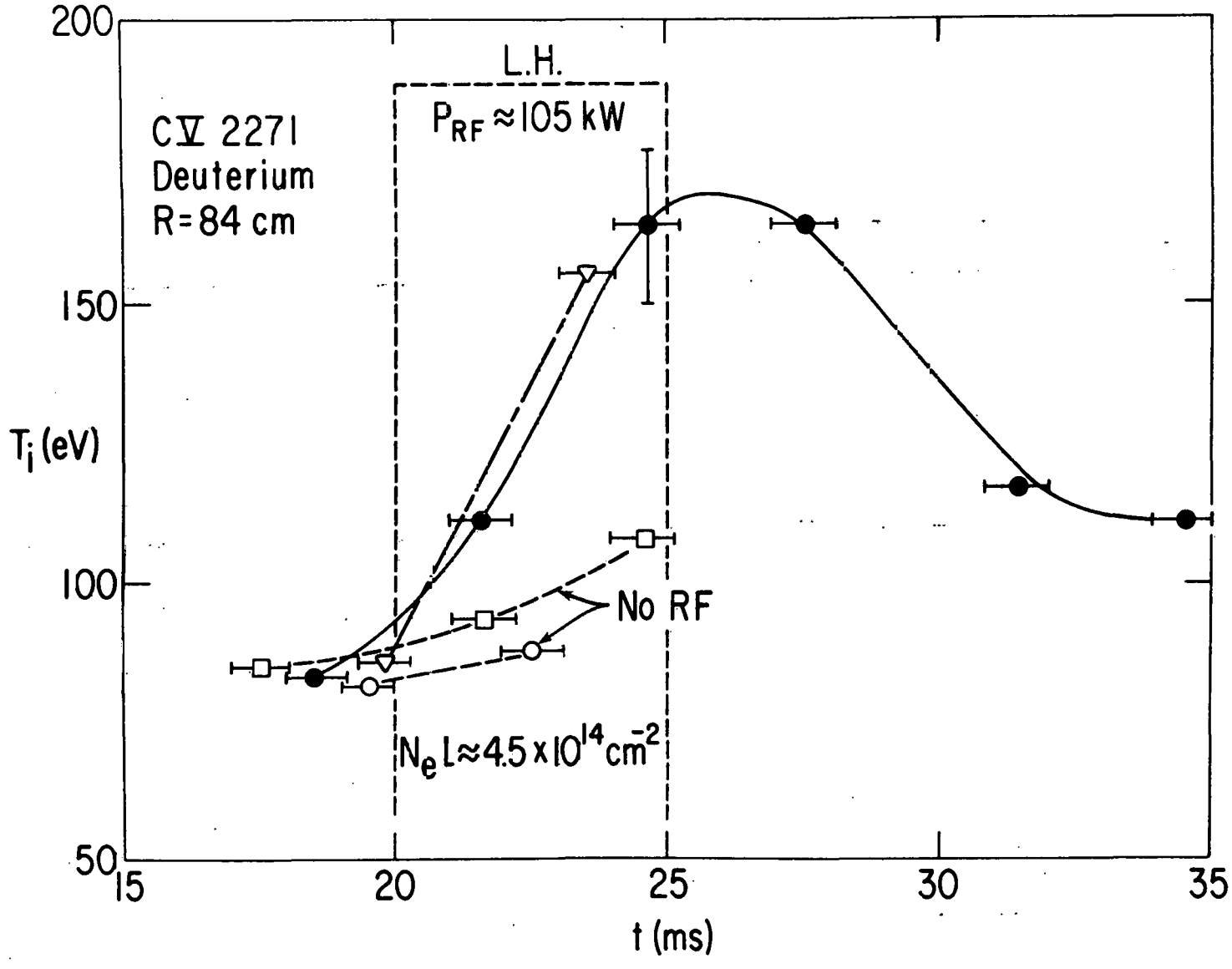
200
150
100
50
L.H.
$P_{RF} \approx 105$ kW
CV 2271
Deuterium
R=84 cm
T_i (eV)
No RF
$N_e L \approx 4.5 \times 10^{14} cm^{-2}$
15
20
25
30
35
t (ms)

766107

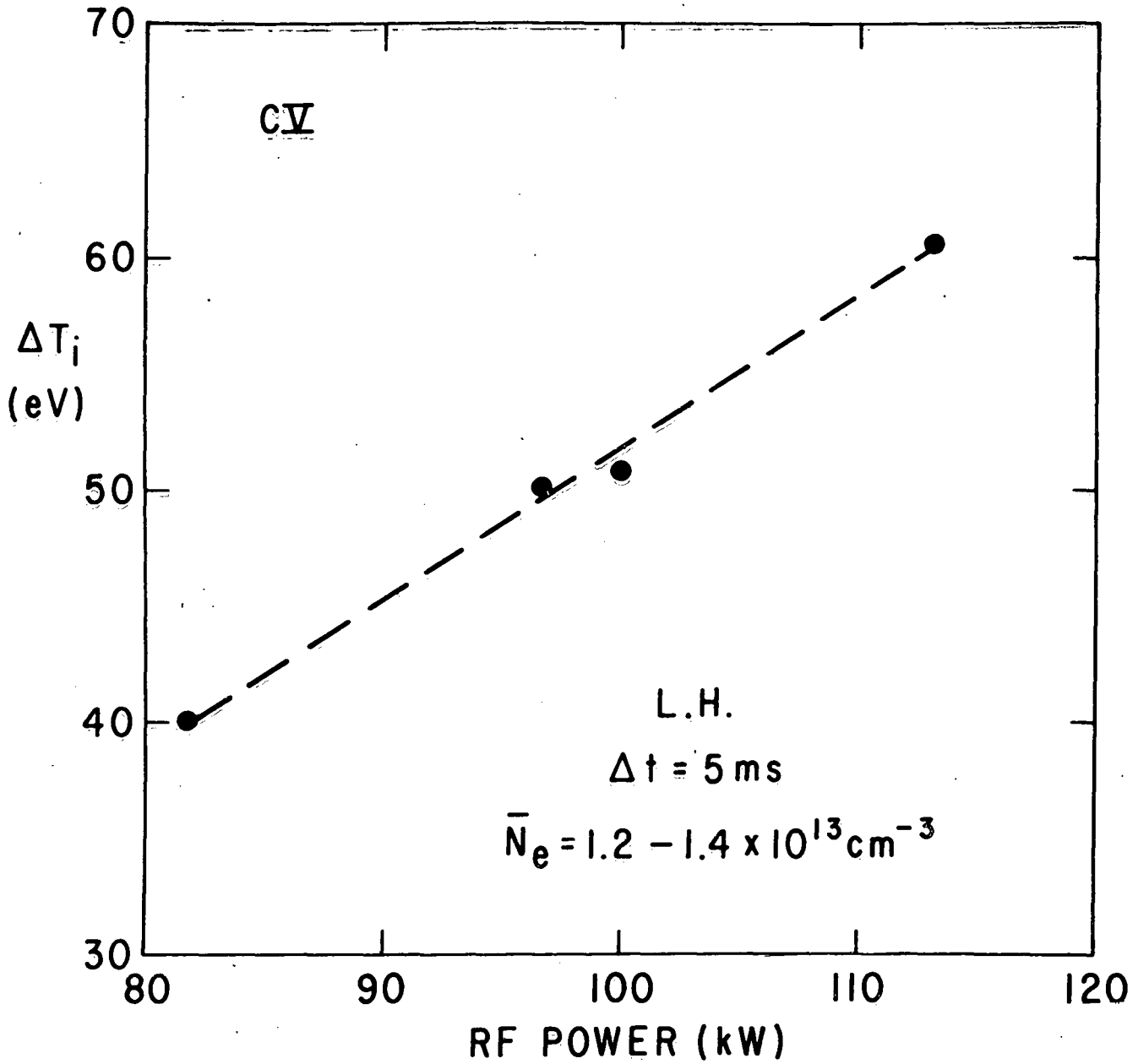

773042

Fig. 8. T_i as a function of RF power (a) and plasma electron density (b) for LH experiments.

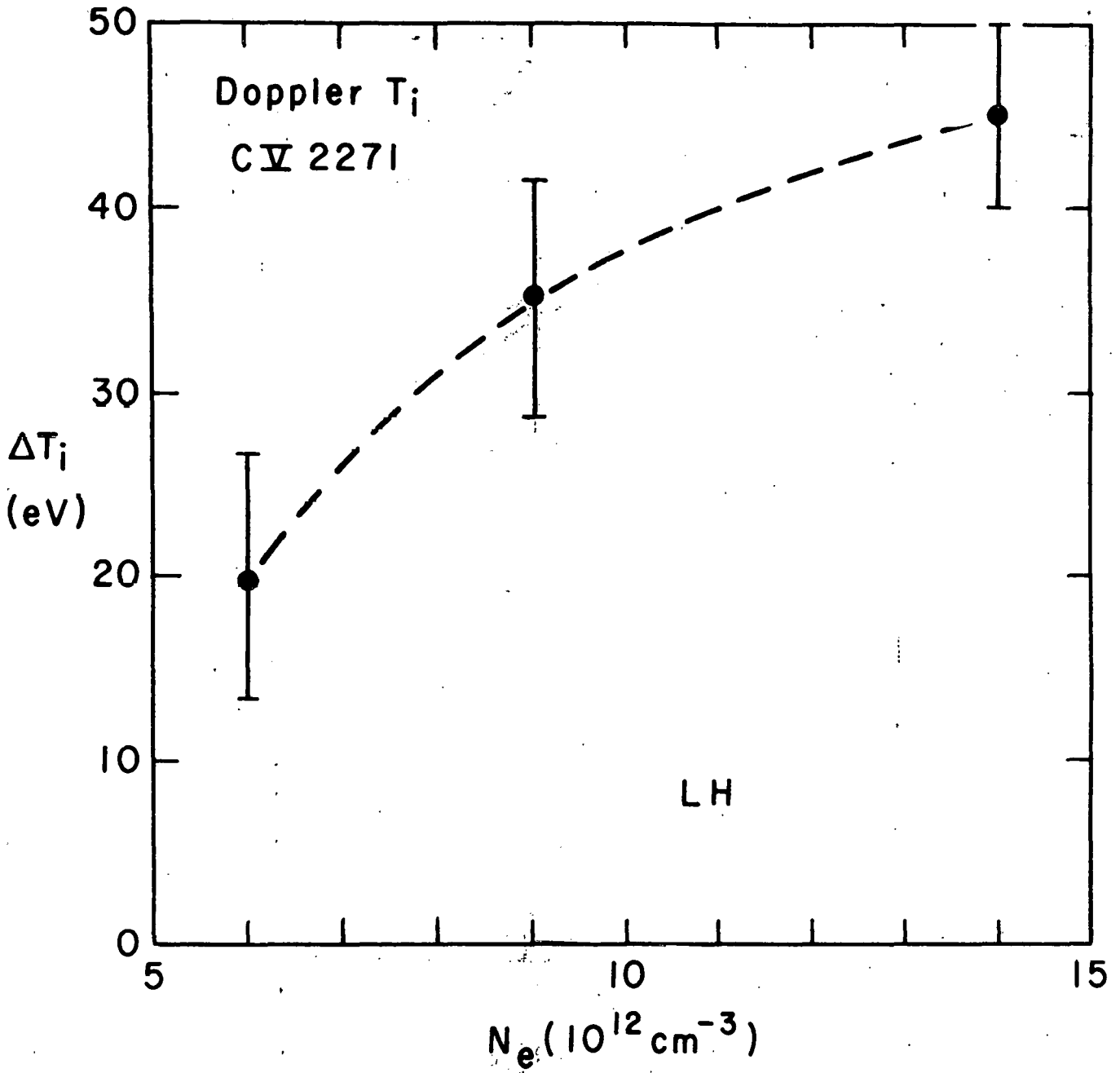
Doppler T_i
C V 2271
LH
ΔT_i (eV)
$N_e(10^{12}cm^{-3})$
0
10
20
30
40
50
5
10
15

773024

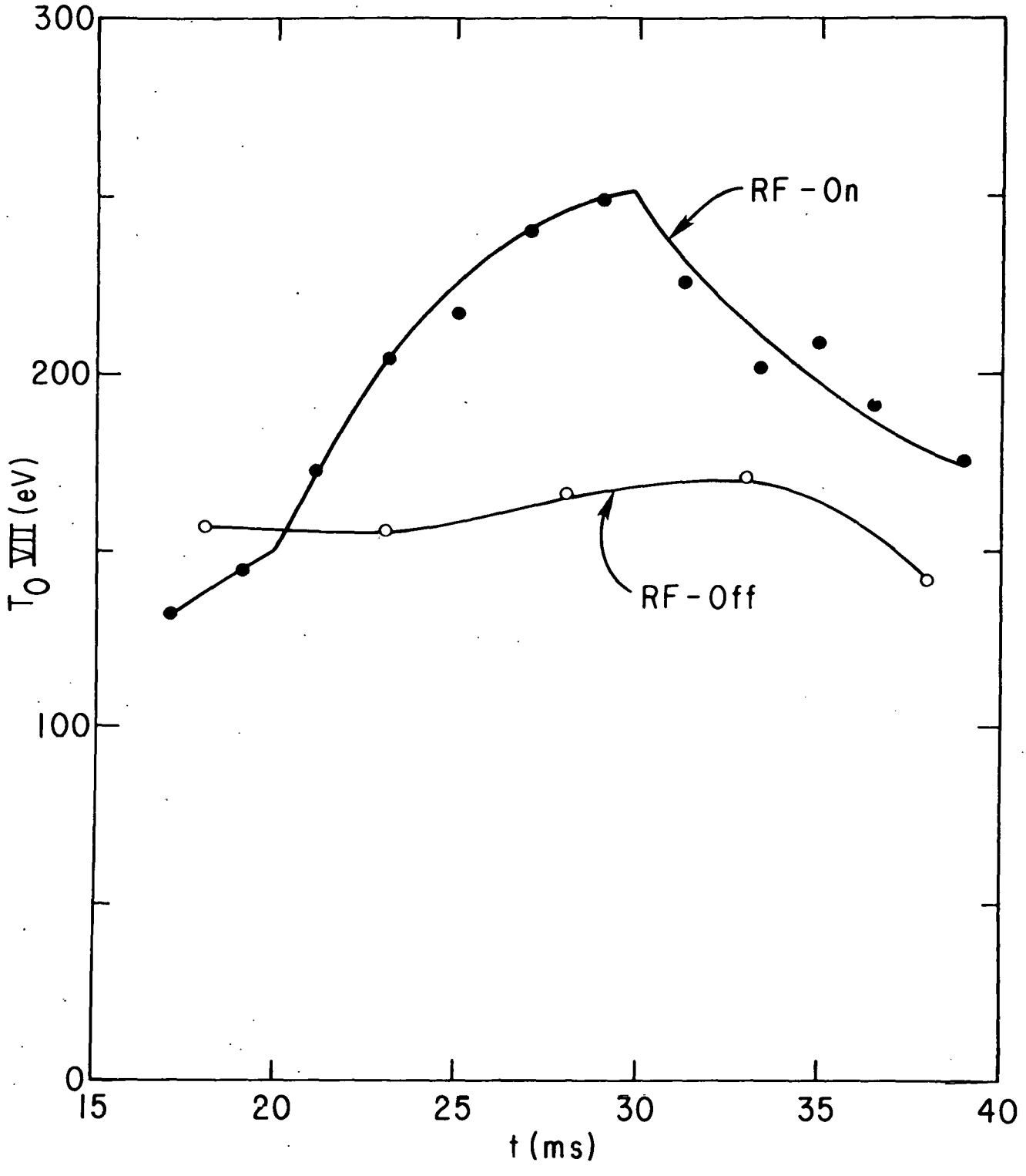

766013

Fig. 9. Doppler T_i (OVII line) during ICRF heating. Lower curve presents result without RF.

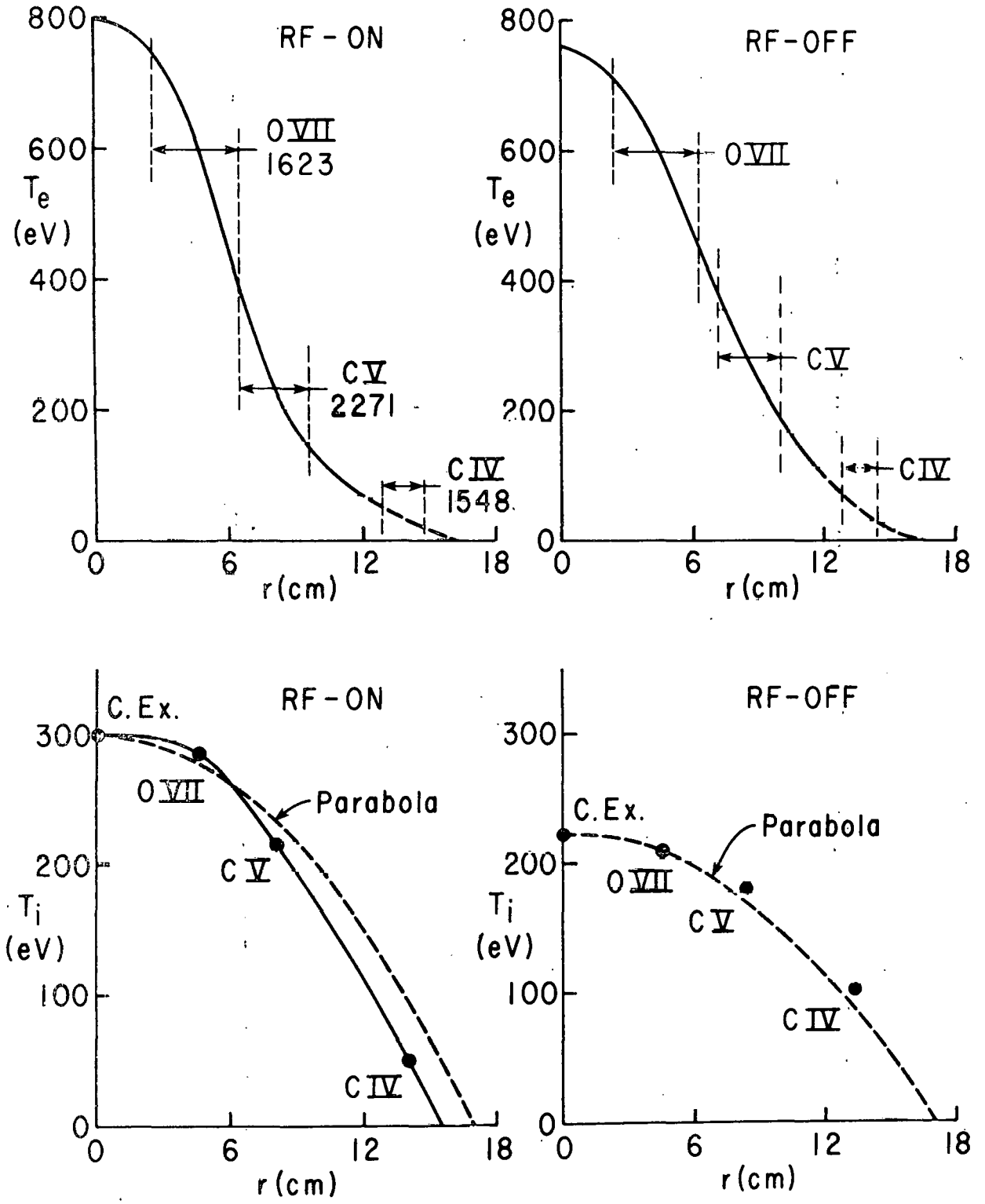

Fig. 10. Ion temperature profiles for ICRF heating experiments (left side). In right side is shown T_i for plasma ohmically heated only. Positions of lines used for measurements are indicated on T_e profiles.

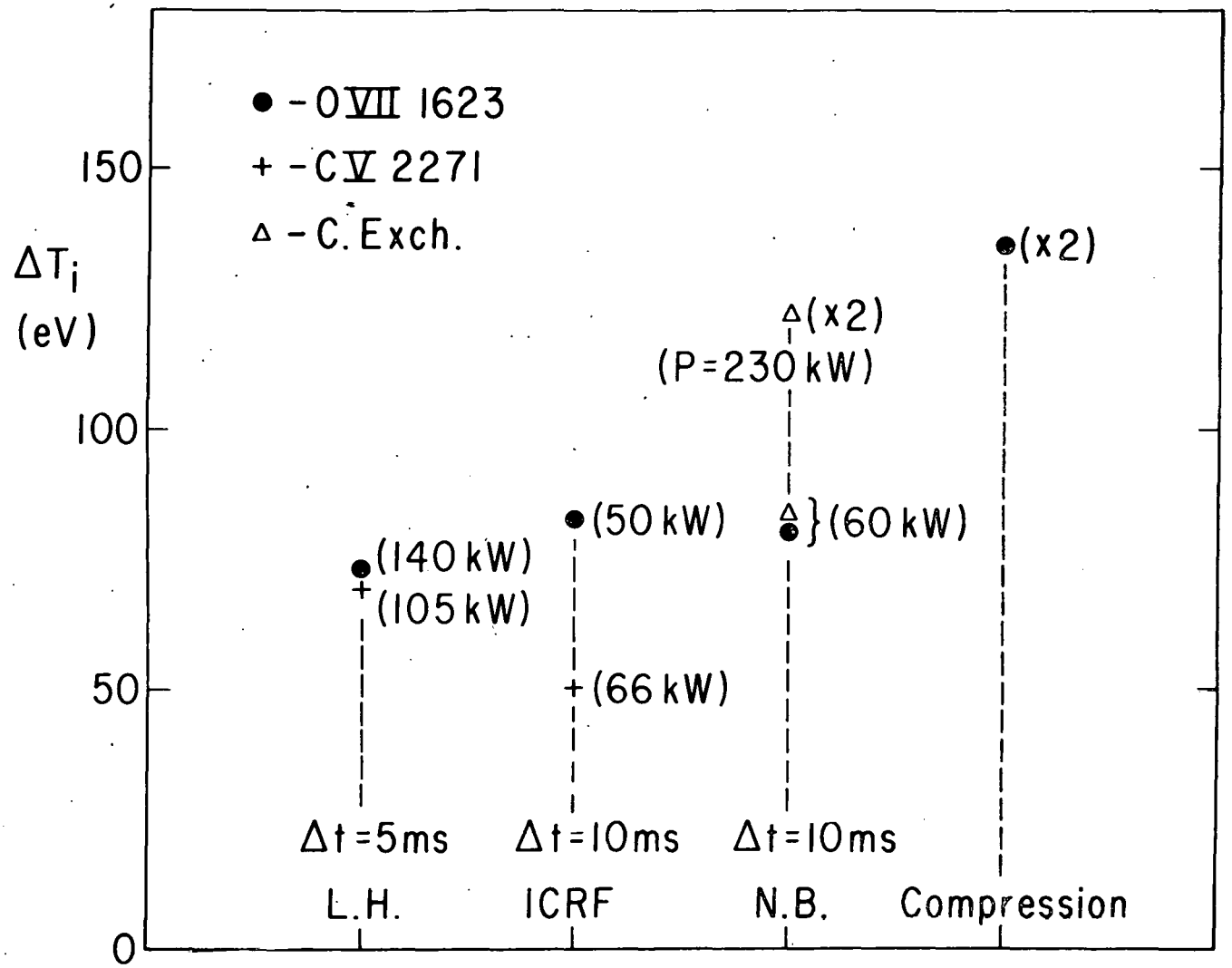

773028

Fig. 11. Observable ΔT_i during supplementary heating experiments and compression. Factor (x2) indicates that given ΔT_i should be read as twice higher. Δt is the duration of the heating pulse.